Observation of coherent oscillations in the association of dimers from a thermal gas of ultracold atoms

Roy Elbaz [ORCID],[1] Yaakov Yudkin,[1] P. Giannakeas,[2] Jan-Michael Rost,[2] Chris H. Greene [ORCID],[3,4] and Lev Khaykovich [ORCID][1]

[1]*Department of Physics, QUEST Center and Institute of Nanotechnology and Advanced Materials,*
Bar-Ilan University, Ramat-Gan 5290002, Israel

[2]*Max Planck Institute for the Physics of Complex Systems, Nöthnitzer Strasse 38, 01187 Dresden, Germany*

[3]*Department of Physics and Astronomy, Purdue University, West Lafayette, Indiana 47907, USA*

[4]*Purdue Quantum Science and Engineering Institute, Purdue University, West Lafayette, Indiana 47907, USA*

We report the observation of coherent oscillations in conversion efficiency of weakly bound dimers formed from a thermal gas of ultracold atoms. Finite thermal energy of the gas causes loss of coherence when a broad continuum is resonantly coupled to a discrete bound state. Restoration of the coherence can be achieved through nonadiabatic transitions of the dressed molecular energy level that are induced by a strong modulation pulse with fast envelope dynamics. Conditions to observe coherent oscillations are verified and control of their properties is demonstrated. The main experimental findings are supported by theoretical modeling and numerical calculations. The observed results may lead to a renewed interest in general studies of a discrete energy level coupled to a broadband continuum when the properties of both are fully controlled.

When coupling between a discrete energy level and a broad continuum is introduced, dynamics is expected to be fully incoherent due to vanishingly short coherent memory of the latter. Numerous quantum electrodynamics systems such as spontaneous emission of an excited atom, photoionization of an atom, and photodissociation of molecules are all fit within the framework of this general scheme [1]. A similar system can be realized with ultracold atoms in the vicinity of collisional resonances which are characterized by the existence of a weakly bound dimer state. An original experimental technique to probe this state was demonstrated in Ref. [2], which consisted of association of dimers from a thermal gas of atoms by modulating the magnetic field bias at a frequency that matches the binding energy. Surprisingly, coherent Rabi-type oscillations in the dimers' conversion efficiency has been reported and remained unexplained since then despite the number of theoretical approaches devoted to the subject [3–7] and despite the straightforward analogy with the above-mentioned systems subject to broadband decoherence mechanisms.

A recent theoretical proposal suggests a mechanism that leads to the restoration of coherence in such a system [8]. Here we carefully explore its conditions and provide the experimental verification. Our studies reveal the crucial importance of fast dynamics initiated by the excitation pulse envelope. The mechanism bares similarities with Stückelberg oscillations demonstrated earlier in multiphoton ionization [9] and in Rydberg excitation [10] of atoms. More recently, similar effect has been suggested theoretically also for x-ray ionization by intense femtosecond laser pulses where their steep rise and fall induces dynamic interference in the photoionization spectra [11–15].

Conversion of ultracold atoms into a weakly bound dimer is executed by modulation of the magnetic field bias $B(t)$ with a resonance frequency ν, as shown in Fig. 1(a). To illustrate the physical mechanism behind the coherent oscillations in the molecule conversion efficiency, the induced interaction dynamics is represented in Fig. 1(b) as a dressed state energy level in the rotating wave approximation. Before the modulation pulse is switched on, the dressed energy level $E_\mathrm{d} + h\nu$ is degenerate with the thermal continuum. When the modulation strength grows, E_d experiences repulsion from the continuum and is pushed down to lower energies. Ultimately, at strong enough modulation $E_d + h\nu$ crosses the dissociation threshold and opens a gap with the continuum [$\Delta_E \gg k_B T$; see Fig. 1(b)]. If the dynamical changes ($\tau_{\mathrm{on,off}}$) of the dressed level are fast compared to timescale set by the thermal energy ($\tau_{\mathrm{th}} = h/k_B T$) the nonadiabatic coupling creates an effective beam splitter each time the threshold is passed and forms a two-path interferometer for a wave function to either make a dimer or remain in an unbound state [see Fig. 1(b)]. As was demonstrated in Ref. [8] such an interferometer should be robust against thermal averaging and, as we show here, it is responsible for the observed coherent oscillations.

Our study settles a long-term quest for a deeper understanding of an experimental technique routinely used for nearly two decades in many species and mixtures such as homo- [16–19] and heteronuclear atomic systems [20–22] and in strongly magnetic atoms [23,24]. Revealing a nonadiabatic effect related to the fast dynamics of the modulation pulse envelope provides an old problem with a fresh perspective and novel and unexpected relations with other systems such as, for example, photoionization with intense femtosecond laser pulses [11–15]. In this context, our work complements and enhances a recently established quantum simulator of ultrafast
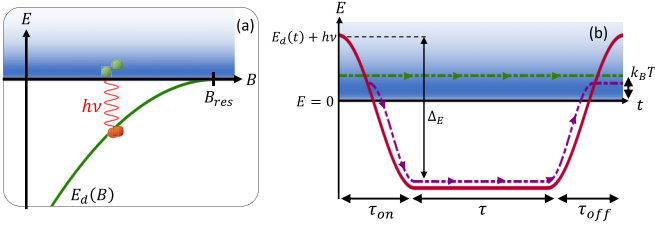
FIG. 1. Schematics of physical mechanisms. (a) Universal dimer energy level in the vicinity of a Feschbach resonance. The binding energy decreases when the magnetic field increases to suit the specifics of the Feshbach resonance used in the experiment. (b) Principles of the interferometer: when the interaction is switched on, fast nonadiabatic transition of the dressed energy level through a thermal atomic ensemble ($\tau_{\mathrm{on,off}} \ll \tau_{\mathrm{th}} = h/k_B T$) splits the wave function into two pathways: one follows the atomic continuum (green dashed-dotted line), while another one follows the bound state shifted below the threshold by strong coupling ($\Delta_E \gg k_B T$). When interaction is switched off the wave function recombines and the outcome depends on the accumulated phase difference between the paths.

phenomena with ultracold atoms [25]. Even in a broader context, our results pave the way for studies of a discrete energy level coupled strongly to a broadband continuum in a well controlled environment provided by ultracold atoms in which both the energy level and the continuum properties can be adjusted.

The experiment is performed in a thermal gas of ^{7}Li atoms, polarized in the $|m_J = -1/2, m_F = 0\rangle$ state and evaporatively cooled to a temperature of $T \approx 1.5\,\mu$K in a crossed-beam optical trap [26]. Feshbach dimers are associated in the vicinity of the 893.78 G s-wave Feshbach resonance by means of a magnetic field modulation at a frequency of $\nu = 2.538$ MHz. The latter is in resonance with the dimer's binding energy when the magnetic field bias is set to 884.94 G, which corresponds to the scattering length $a = 425 a_0$ [18,27]. The modulation is applied by two auxiliary coils on both sides of the vacuum chamber, aligned with the magnetic-field bias.

In the first set of experiments we explore the effect of large modulation amplitudes b_0 on the dimer binding energy. Up to a second order in perturbation theory the dimer energy (averaged over a modulation period) is expressed as a dressed state [28]:

$$E_d(b_0) \approx A E_{\mathrm{bare}}\left[1 + \frac{3}{2A}\left(\frac{b_0}{B_{\mathrm{bare}} - B_{\mathrm{res}}} \right)^2 \right], \quad (1)$$

where $E_{\mathrm{bare}} = -\hbar^2/m a_{\mathrm{bare}}^2$ is the dimer binding energy for vanishing modulation strength in the universal limit, $a_{\mathrm{bare}} = |a_{bg}\Delta/(B_{\mathrm{bare}} - B_{\mathrm{res}})|$ and B_{bare} are the corresponding scattering length and magnetic field, Δ and B_{res} are the width and location of the Feshbach resonance, and $A \approx 0.86$ corrects E_{bare} for the finite range of the potential and the resonance strength. When the modulation frequency ν satisfies the resonance condition, i.e., $E_d = h\nu$, dimers are formed most efficiently [2]. Thus characterizing the optimal dimer conversion efficiency as a function of modulation strength and using Eq. (1) allows for accurate calibration of b_0 at the position
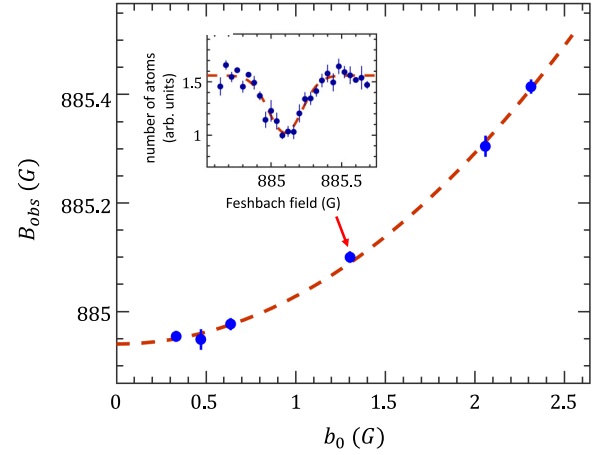

FIG. 2. Shift in resonance. Optimal bias field for dimer association B_{obs} as a function of the magnetic field modulation amplitude b_0. Each blue data point stands for a dimer association spectroscopy loss measurement. The dashed red curve is drawn according to Eq. (2) [28]. In the inset an example for such a spectroscopy measurement is shown, where the remaining number of atoms in the trap after the rf pulse of a fixed frequency ν is plotted versus the bias magnetic field.

of atoms. This information is important to verify the first condition to observe Stückelberg oscillations.

In the experiment the modulation frequency is fixed and we scan the magnetic-field bias to find the resonance response in dimer association. Recasting Eq. (1) in this language we get

$$|B_{\mathrm{obs}} - B_{\mathrm{res}}| \approx \sqrt{A}|B_{\mathrm{bare}} - B_{\mathrm{res}}|\left[1 + \frac{3}{4A}\left(\frac{b_0}{B_{\mathrm{bare}} - B_{\mathrm{res}}} \right)^2 \right]. \quad (2)$$

For each value of b_0 we scan the magnetic-field bias and measure the number of remaining atoms in the trap after a short waiting time during which the molecules decay from the trap due to inelastic collisions [see Fig. 2 (inset)]. The pulse duration is varied from 150 μs to 500 μs to keep the loss contrast [($N_{\mathrm{bg}} - N_{\mathrm{min}})/N_{\mathrm{bg}}$, where $N_{\mathrm{bg,min}}$ is the background and the minimal number of atoms] roughly constant and ∼40%. The resulting loss resonance is fitted with a Gaussian profile and the center value B_{obs} is extracted. In Fig. 2 B_{obs} is shown as a function of b_0 revealing that a maximal shift of $B_{\mathrm{obs}} - B_{\mathrm{bare}} = 466$ mG can be readily obtained with a modulation amplitude as large as $b_0 = 2.3$ G at the position of atoms [28]. This corresponds to an energy shift of $\Delta_E \approx h \times 260$ kHz, which surpasses the thermal energy by almost one order of magnitude and satisfies the condition to observe Stückelberg oscillations. Note that having this large energy margin is essential for the success of the experimental demonstration as will be clarified below.

Consider next the main experimental protocol used for the observation of the Stückelberg oscillations. The modulation coils are part of a resonant RLC circuit to maximize the available modulation amplitude. This results into a time-dependent magnetic field of the following form:

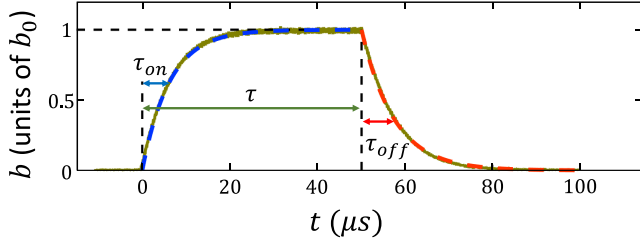$$B(t) = B + b(t)\sin(2\pi \nu t), \quad (3)$$

FIG. 3. Modulation pulse envelope. The magnetic field modulation envelope is shown together with fitting to Eq. (4). The pulse is turned on at $t = 0$ for a duration τ (blue dashed line) and is turned off at $t = \tau$ (red dashed line). The rise and fall times $\tau_{\mathrm{on,off}}$ are marked by blue and red double arrows, respectively. The maximal pulse amplitude, denoted by b_0, is reached for $\tau \gg \tau_{\mathrm{on}}$.

where $b(t)$ is the pulse envelope described by the relation

$$b(t) = \begin{cases} b_0[1 - \exp(-t/\tau_{\mathrm{on}})], & 0 \leqslant t < \tau, \\ b_1 \exp[-(t - \tau)/\tau_{\mathrm{off}}], & t \geqslant \tau, \end{cases} \quad (4)$$

where τ is the pulse duration, $b_1 = b_0[1 - \exp(-\tau/\tau_{\mathrm{on}})]$ is the amplitude at the moment the pulse is switched off, and $\tau_{\mathrm{on,off}}$ are the rise and fall times of the pulse envelope. Figure 3 shows the pulse's envelope as measured by a pick-up antenna. By fitting it to Eq. (4) the rise and fall times are extracted to be $\tau_{\mathrm{on}} = 6.27\ \mu s$ and $\tau_{\mathrm{off}} = 7.38\ \mu s$. Note that the typical timescale of the system attributed to the finite thermal energy is longer than the envelope's dynamics ($\tau_{\mathrm{th}} \approx 30\ \mu s > \tau_{\mathrm{on,off}}$)

satisfying the nonadiabaticity criterion [see Fig. 1(b)]. The dressed energy level dynamics $E_d(t)$ is now described by Eq. (1) where b_0 is substituted with $b(t)$.

Before the modulation pulse is turned on, a bias field B is applied, such that $h\nu > |E_{\mathrm{bare}}|$. As the pulse is turned on $E_d(t)$ is shifted to lower values and when the pulse is turned off the energy level goes back to its initial value. We explore three different scenarios illustrated in Fig. 4(a). They differ from each other only by the applied bias field $B^{(i)}$ ($i \in \{i,ii,iii\}$), so that although the initial energies $E_d(t = 0)$ are different, the modulation amplitude b_0 remains the same for all scenarios. This approach assures minimal changes in the experimental conditions which is less so if, for example, the pulse intensity is varied instead. To keep the validity of nonadiabaticity in all scenarios we start above the threshold with at least $\sim 2k_B T$ [see Fig. 4(a)]. This forces the dressed dimer energy level to pass the majority of populated continuum rapidly and is especially relevant to avoid the problematic long tail of weak modulation when the pulse is switched off (see the red dashed tail in Fig. 3).

For the scenarios (ii) and (iii) we expect Stückelberg oscillations in dimer conversion efficiency. When the pulse amplitude starts to grow the initial nonadiabatic passage of the dressed energy level through the continuum imitates the entrance beam splitter of an interferometer at which the initial wave function splits between the free atoms and the bound state pathways. As the pulse amplitude continues to grow, the two paths decouple and accumulate a dynamic phase differ-
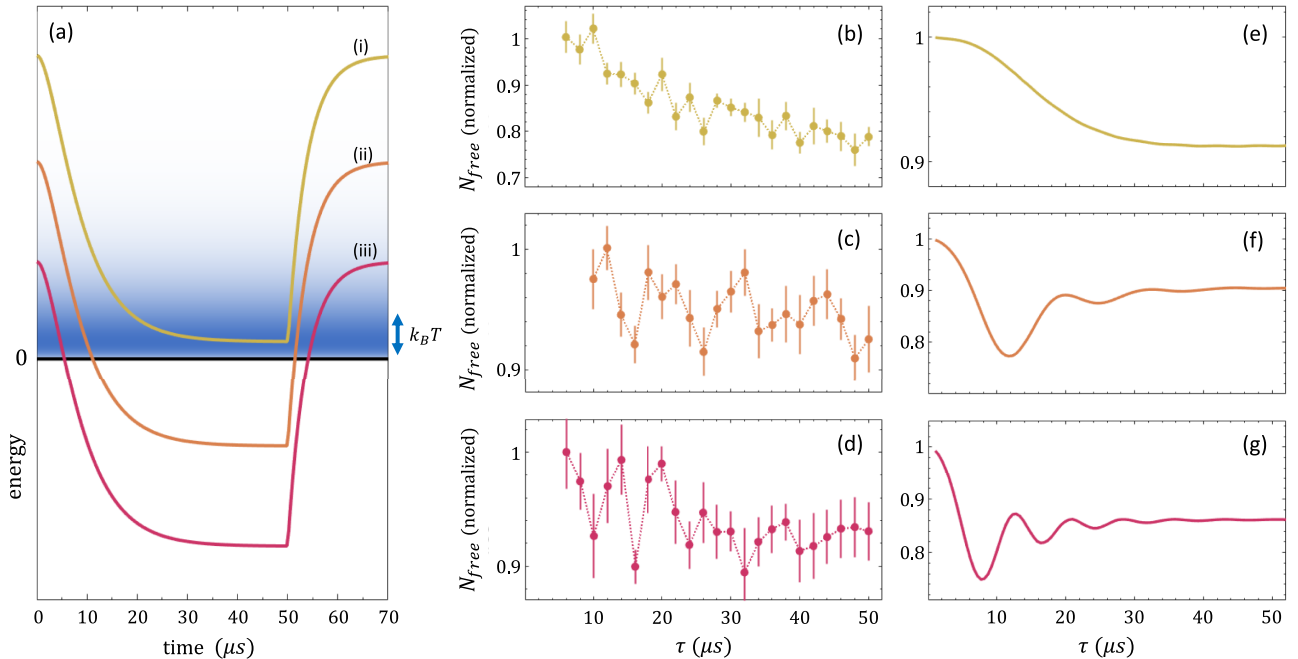

FIG. 4. Experimental results and numerical calculations. (a) Time evolution of the dressed dimer energy level $E_d(t) + h\nu$ as the modulation pulse is applied. The initial energy at $t = 0$ is different for the three scenarios. The thermal population of free atoms is gradiated by the blue color gradient with an energy width of $k_B T$. Cases (i), (ii), and (iii) are marked in yellow, orange, and red solid lines, respectively. Panel (b) shows the remaining number of free atoms in the trap for different modulation pulse durations τ corresponding to the case (i) in which the dimer is in resonance with the continuum when the pulse is at its maximal modulation amplitude. Panels (c) and (d) show the same plot for cases (ii) and (iii), respectively, where Stückelberg oscillations are visible. Panels (e)–(g) show corresponding numerical calculations as per Ref. [8] with parameters suitable for our experimental realization.

ence according to their energy separation. When the pulse is turned off the dressed dimer level crosses the continuum again, this time imitating the exit beam splitter at which the two pathways of the wave function recombine. The resulting interference is measured through counting the number of free atoms as a function of pulse duration τ (see Fig. 3). Note that the population of the dimer state is hidden in the dark because, prior to detection, the magnetic-field bias is shifted to deepen the dimer binding energy to ~ 6 MHz. Thus the bound state remains decoupled from the weak, on-resonance detection light. In the first scenario (i) of Fig. 4(a) the dynamics is mostly adiabatic for energies near $k_B T$, which efficiently eliminates the entrance beam splitter. Although the exit beam splitter is still created by the sharp end of the pulse, Stückelberg oscillations are not expected in this case.

The experimental results and the corresponding numerical calculations based on the integration of the time-dependent Schrödinger equation are shown in Figs. 4(b)–4(d) and 4(e)–4(g), respectively. Each data point is an average of 16–32 runs and the error bars signify the standard deviation. All measurements are performed with the maximal modulation amplitude of $b_0 = 2.3$ G. The numerics are done according to prescriptions of Ref. [8] with parameters suitable for our experimental realization and they show qualitative agreement with the measurements (for details see [28]). Quantitative discrepancies are discussed at the end of this section.

In case (i), shown in Fig. 4(b), the bias field is set to $B^{(i)} = B_{obs}(b_0 = 2.3$ G) (see Fig. 2) and the dressed level becomes resonant with the continuum only when the pulse amplitude reaches its maximum. The interferometric sequence is not realized in this case which can be identified in the monotonic decrease in the number of atoms as a function of pulse duration τ. For $\tau < 10$ μs and $\tau > 40$ μs, the signal agrees with static saturation. In the former case the pulse amplitude is still weak and the modulation frequency is off resonance as can be seen in Fig. 4(a), keeping the production efficiency low. The latter is obtained when the rates of association and dissociation of dimers due to on-resonance modulation become equal. Similar behavior can be identified in the numerical calculations shown in Fig. 4(e).

In case (ii), shown in Fig. 4(c), the bias field is set to $B^{(ii)} = B_{obs}(b_0 = 1.45$ G). Since now the initial dimer energy is lower, the dressed dimer level crosses the threshold and reaches a separation with the continuum [Fig. 4(a)]. The oscillations are visible here with two minima and two maxima that can be readily identified and they agree with a frequency of ~ 80 kHz supported by the numerical calculations shown in Fig. 4(f). At longer times the oscillations wash out in both experiment and theory due to the broadband continuum [8].

Case (iii) is shown in Fig. 4(d) for which the bias field is set to $B^{(iii)} = B_{obs}(b_0 = 0.77$ G). As the dressed dimer energy opens a larger gap with the continuum, a faster oscillation frequency is observed. Also here two minima and two maxima can be identified and their frequency agrees with ~ 110 kHz. Figure 4(g) shows the corresponding numerical calculations and confirms a faster oscillation frequency. Note, however, that the frequency is not constant. Close examination of both experimental and theoretical curves shows that the short-time

dynamics is somewhat slower. This is because for $\tau \lesssim \tau_{on}$ the pulse amplitude $b(t)$ does not reach its maximal value b_0 and the opened gap is therefore smaller.

Although numerical calculations qualitatively agree with the experimental measurements, quantitative discrepancies are visible. The largest discrepancy can be associated with the signals' contrasts. For example, for incoherent dimer production the theory underestimates the production efficiency by about a factor of two. It can be partially compensated by the fact that the numerical calculations neglect inelastic losses of dimers. While this assumption is correct for all pulse durations used here, in the experiment more time passes between the end of the pulse and the detection during which the majority of dimers are lost. As the dominant loss mechanism involves inelastic collisions between a dimer and a free atom, the measured number of atoms should be smaller by a factor of ~ 1.5. Although in this case the agreement would improve, for other sets of measurements the oscillation contrast in the numerical calculations is larger by a factor of ~ 3 (for the first oscillation) and the inclusion of losses will only increase this discrepancy.

We believe that the main disagreement comes from the fact that the numerical calculations are performed with a zero-range model where the universal dimer energies are matched with those obtained from the experimental measurements. Although we work with the scattering length an order of magnitude larger than the van der Waals length of the interatomic potential, the details of the true potential are already responsible for deviation of the binding energy from the universal formula [18,28]. Thus these details play a role in dimer association especially for short pulse durations ($\sim$μs) for which the bandwidth is comparable to the energy gap between the dressed state and the continuum threshold. Note also that Feshbach resonances in ^{7}Li are all narrow in character [27], which makes a single channel approach less reliable.

In conclusion, a robust coherent phenomenon in the conversion efficiency of Feshbach dimers formed from a thermal gas of ultracold atoms has been experimentally demonstrated and compared with theory. Our proof of concept studies can be improved in many ways. Access to lower temperatures, limited by technical reasons, should improve the contrast of oscillations and allow the study of decoherence rates in the system. This, in turn, opens the way to extend the system to more complex scenarios and to address questions regarding the environment influence on the observed coherent phenomenon. If the density is increased elastic and inelastic collisions between the superposition state constituents might set in and cause collisional broadening or narrowing which can be revealed via measuring decoherence rates as a function of density. Such adjustability of the continuum is an excellent example for the control the platform of ultracold atoms can provide for the system under study.

[1] C. Cohen-Tannoudji, J. Dupont-Roc, and G. Grynberg, *Atom-Photon Interactions: Basic Process and Applications* (Wiley-VCH, Weinheim, 2004).

[2] S. P. Thompson, E. Hodby, and C. E. Wieman, Ultracold Molecule Production via a Resonant Oscillating Magnetic Field, Phys. Rev. Lett. **95**, 190404 (2005).

[3] T. M. Hanna, T. Köhler, and K. Burnett, Association of molecules using a resonantly modulated magnetic field, Phys. Rev. A **75**, 013606 (2007).

[4] B. Bazak, E. Liverts, and N. Barnea, Multipole analysis of radio-frequency reactions in ultracold atoms, Phys. Rev. A **86**, 043611 (2012).

[5] S. Brouard and J. Plata, Feshbach molecule formation through an oscillating magnetic field: Subharmonic resonances, J. Phys. B: At., Mol., Opt. Phys. **48**, 065002 (2015).

[6] C. Langmack, D. Hudson Smith, and E. Braaten, Association of Atoms into Universal Dimers Using an Oscillating Magnetic Field, Phys. Rev. Lett. **114**, 103002 (2015).

[7] A. Mohapatra and E. Braaten, Harmonic and subharmonic association of universal dimers in a thermal gas, Phys. Rev. A **92**, 013425 (2015).

[8] P. Giannakeas, L. Khaykovich, J.-M. Rost, and C. H. Greene, Non-Adiabatic Molecular Association in Thermal Gases Driven by Radio-Frequency Pulses, Phys. Rev. Lett. **123**, 043204 (2019).

[9] R. R. Jones, Interference Effects in the Multiphoton Ionization of Sodium, Phys. Rev. Lett. **74**, 1091 (1995).

[10] U. Bengs, S. Patchkovskii, M. Ivanov, and N. Zhavoronkov, All-optical Stückelberg spectroscopy of strongly driven Rydberg states, Phys. Rev. Res. **4**, 023135 (2022).

[11] P. V. Demekhin and L. S. Cederbaum, Dynamic Interference of Photoelectrons Produced by High-Frequency Laser Pulses, Phys. Rev. Lett. **108**, 253001 (2012).

[12] K. Toyota, U. Saalmann, and J.-M. Rost, The envelope Hamiltonian for electron interaction with ultrashort pulses, New J. Phys. **17**, 073005 (2015).

[13] M. Baghery, U. Saalmann, and J.-M. Rost, Essential Conditions for Dynamic Interference, Phys. Rev. Lett. **118**, 143202 (2017).

[14] Q.-C. Ning, U. Saalmann, and J.-M. Rost, Electron Dynamics Driven by Light-Pulse Derivatives, Phys. Rev. Lett. **120**, 033203 (2018).

[15] Note that [11] contains flaws in the theoretical and numerical results; see [13].

[16] S. B. Papp and C. E. Wieman, Observation of Heteronuclear Feshbach Molecules from a ^{85}Rb − ^{85}Rb Gas, Phys. Rev. Lett. **97**, 180404 (2006).

[17] A. D. Lange, K. Pilch, A. Prantner, F. Ferlaino, B. Engeser, H.-C. Nägerl, R. Grimm, and C. Chin, Determination of atomic scattering lengths from measurements of molecular binding energies near Feshbach resonances, Phys. Rev. A **79**, 013622 (2009).

[18] N. Gross, Z. Shotan, O. Machtey, S. J. J. M. F. Kokkelmans, and L. Khaykovich, Study of Efimov physics in two nuclear-spin sublevels of ^{7}Li, C. R. Phys. **12**, 4 (2011).

[19] P. Dyke, S. E. Pollack, and R. G. Hulet, Finite-range corrections near a Feshbach resonance and their role in the Efimov effect, Phys. Rev. A **88**, 023625 (2013).

[20] J. P. Gaebler, J. T. Stewart, J. L. Bohn, and D. S. Jin, p-Wave Feshbach Molecules, Phys. Rev. Lett. **98**, 200403 (2007).

[21] C. Weber, G. Barontini, J. Catani, G. Thalhammer, M. Inguscio, and F. Minardi, Association of ultracold double-species bosonic molecules, Phys. Rev. A **78**, 061601(R) (2008).

[22] F. Wang, X. He, X. Li, B. Zhu, J. Chen, and D. Wang, Formation of ultracold NaRb Feshbach molecules, New J. Phys. **17**, 035003 (2015).

[23] A. Frisch, M. Mark, K. Aikawa, S. Baier, R. Grimm, A. Petrov, S. Kotochigova, G. Quéméner, M. Lepers, O. Dulieu, and F. Ferlaino, Ultracold Dipolar Molecules Composed of Strongly Magnetic Atoms, Phys. Rev. Lett. **115**, 203201 (2015).

[24] Z.-X. Ye, A. Canali, E. Soave, M. Kreyer, Y. Yudkin, C. Ravensbergen, E. Kirilov, and R. Grimm, Observation of low-field Feshbach resonances between ^{161}Dy and ^{40}K, Phys. Rev. A **106**, 043314 (2022).

[25] R. Senaratne, S. V. Rajagopal, T. Shimasaki, P. E. Dotti, K. M. Fujiwara, K. Singh, Z. A. Geiger, and D. M. Weld, Quantum simulation of ultrafast dynamics using trapped ultracold atoms, Nat. Commun. **9**, 2065 (2018).

[26] N. Gross and L. Khaykovich, All optical production of ^{7}Li Bose-Einstein condensation using Feshbach resonances, Phys. Rev. A **77**, 023604 (2008).

[27] P. S. Julienne and J. M. Hutson, Contrasting the wide Feshbach resonances in ^{6}Li and ^{7}Li, Phys. Rev. A **89**, 052715 (2014).

[28] See Supplemental Material at http://link.aps.org/supplemental/10.1103/PhysRevA.107.L031304, which includes Ref. [29], for the experimental details explaining Fig. 2, notes on derivation of Eqs. (1) and (2), likelihood analysis of the data, and clarifications on the theoretical model.

[29] C. Chin, R. Grimm, P. Julienne, and E. Tiesinga, Feshbach resonances in ultracold gases, Rev. Mod. Phys. **82**, 1225 (2010).